Deka-keV X-ray observations of solar bursts with WATCH/GRANAT: frequency distributions of burst parameters

N. Crosby, N. Vilmer, N. Lund, R. Sunyaev

Astron. Astrophys. 334, 299–313 (1998)

ASTRONOMY
AND
ASTROPHYSICS

Deka-keV X-ray observations of solar bursts with WATCH/GRANAT: frequency distributions of burst parameters

N. Crosby[1,2], **N. Vilmer**[1], **N. Lund**[3], **and R. Sunyaev**[4]

[1] LPSH, URA 2080 CNRS, DASOP Observatoire de Paris, Section d'Astrophysique de Meudon, 5, Place J. Janssen, F-92195 Meudon Cedex, France
[2] LPCE, UPR 4010 du CNRS, conventionee avec l'Universite d'Orleans, 3A, Avenue de la Recherche Scientifique, F- 45071 Orléans la Source Cedex 2, France
[3] Danish Space Research Institute, Juliane Maries Vej 30, DK-2100 Copenhagen, Denmark
[4] Space Research Institute, Profsoyuznaja 84/32, 117296 Moscow, Russia

Received 22 July 1997 / Accepted 18 November 1997

Abstract. Solar flare observations in the deka-keV range are performed by the WATCH experiment on board the GRANAT satellite. The WATCH experiment is presented, including the energy calibration as applied in the present work. The creation of the solar burst catalogue covering two years of observation is described and some examples of solar observations are given. The estimated energy releases in the flares presented here are found to extend below the range of hard X-ray flares which were previously studied by ISEE-3 and HXRBS/SMM detectors. The X-ray emitting component cannot be exclusively explained by contributions from a thermal plasma around a few keV. Either a hotter component or a non-thermal population of particles must also be present to produce the observed deka-keV emission. The WATCH data furthermore shows that the relative contributions of these components may change during an event or from event to event and that the injection of energy contained in suprathermal electrons may occur throughout an event and not only during the rise phase. For the most energetic WATCH flares simultaneous observations performed by other experiments at higher energies further indicate that non-thermal emission can be observed as low as 10 keV. A statistical study is performed on the total WATCH solar database and frequency distributions are built on measured X-ray flare parameters. It is also investigated how the properties of these frequency distributions behave when subgroups of events defined by different ranges of parameters are considered. No correlation is found between the elapsed time interval between successive flares arising from the same active region and the peak intensity of the flare.

Key words: Sun: activity – Sun: flares – Sun: X-rays, gamma rays

Send offprint requests to: N. Crosby

1. Introduction

It is well known that the solar corona is a very dynamic region which is the seat of many phenomena related to magnetic energy releases in a large range of sizes and occurring on time scales going from a few seconds or less to hours. Physical processes leading to magnetic energy releases have been analyzed in individual solar flares using multi-wavelength observations. Such single-case studies constrain the number and energy spectrum of accelerated electrons and ions and the characteristics of magnetic structures at different scales in which energetic particles are produced, propagate and radiate.

The statistical behaviour of solar flares has been characterized with frequency distributions of hard X-ray parameters (Datlowe et al. 1974; Lin et al. 1984; Dennis 1985; Schwartz et al. 1992; Crosby et al. 1993; Lee et al. 1993; Pearce et al. 1993; Bai 1993; Biesecker 1994; Biesecker et al. 1994; Bromund et al. 1995; Lee et al. 1995; Kucera et al. 1997). It is found that most of the distributions can be represented by power-laws having a slope ranging from -2.4 and -1.4 above a threshold (usually attributed to the sensitivity of the experiment used), (see Crosby (1996) for a review).

The most recent statistical studies were based on hard X-ray data originating from long-term solar flare observations obtained with the Hard X-Ray Burst Spectrometer (HXRBS) on the Solar Maximum Mission (SMM) spacecraft (Crosby et al. 1993) and by the X-ray spectrometer aboard the International Cometary Explorer (ICE, formerly known as ISEE 3) spacecraft (Bromund et al. 1995). The measured parameters are the peak count rate (C), the total duration (D) and the peak photon flux (F). The peak energy flux (E) and the total energy (W) in accelerated electrons were also computed using a single power-law photon spectrum and a thick-target interaction model. The slopes of the power-law distributions computed above a threshold are summarized for both studies in Table 1. Power-law distributions are found to extend for several decades. The slopes deduced by Bromund et al. (1995) are found to be slightly steeper

Table 1. Characteristics of the occurrence distributions of HXR flare parameters

	C ($c\ s^{-1}$)	D (s)	F ($ph\ cm^{-2}\ s^{-1}$)	E ($ergs\ s^{-1}$)	W (ergs)
HXRBS/SMM (Crosby et al., 1993)					
slope	-1.73+/-0.01	-2.17+/-0.05	-1.59+/-0.01	-1.67+/-0.04	-1.53+/-0.02
threshold	30 $c\ s^{-1}$	200 s	1.5 $ph\ cm^{-2}\ s^{-1}$	10^{27} $ergs\ s^{-1}$	3×10^{28} ergs
ISEE-3 (Bromund et al., 1995)					
slope	-	-2.40+/-0.04	-1.86+/-0.01	-1.92+/-0.02	-1.67+/-0.02
threshold	-	100 s	4 $ph\ cm^{-2}s^{-1}$	2×10^{27} $ergs\ s^{-1}$	10^{29} ergs

than the ones deduced by Crosby et al (1993). This may be due to differences in instrument sensitivity for the measured parameters or to different methods of estimating electron energy for computed parameters. It was pointed out by Crosby et al. (1993) that the distribution in photon flux obtained for the microflares observed by Lin et al. (1984) closely agrees with the extrapolated distribution of all flares observed near solar maximum. This strengthens the assumption that the deviation from the power-law observed below the threshold of 1.5 $ph\ cm^{-2}\ s^{-1}$ with HXRBS/SMM reflects only the effect of the instrumental sensitivity threshold. On the other hand it has been noticed that there seems to be a deficiency of stronger/longer events seen in the frequency distributions of durations and fluxes. It is possible that this may be due to an observational effect (data gaps, saturation) but as suggested by Lu et al. (1993), it cannot be excluded that this effect may be real.

Another statistical study was performed on the HXRBS/SMM data by Pearce et al. (1993) leading to similar results for the distribution in peak count rates as in Crosby et al. (1993). They furthermore studied the distribution of the time intervals between consecutive HXRBS events (limited to the 60 minute spacecraft day) and found that the flares did not seem to be randomly distributed in time, but that the occurrence distribution of time intervals was best fitted by a power-law distribution. Similar results were also found using observations from BATSE (Biesecker 1994). More recently (Kucera et al. 1997) studied if the frequency distribution of HXRBS/SMM flares varies as a function of the size of the active region. Basically they find that fewer large flares are produced by active regions with small total sunspot area and that large complex regions appear to produce a lower percentage of low energy flares than smaller, simpler regions.

In the soft X-ray domain, frequency distributions of global soft X-ray parameters are also found (Hudson et al. 1969; Drake, 1971; Lee et al. 1995; Shimizu 1994, 1995) to be all well-represented by power-laws with slopes ranging from -1.4 to -2.5. Shimizu (1994, 1995) performed frequency distributions on the estimated energy content of transient brightenings measured by the soft X-ray telescope aboard YOHKOH in the 0.4-4.0 keV range. He found that the distributions can be represented by a single power-law with a slope $\sim$ -1.5, -1.6, which is similar to what has been found for energy distributions in the hard X-ray range. This may suggest that independently of the form under which the released energy is converted (plasma heating or production of non-thermal particles), frequency distributions of total energy contained in either non-thermal particles or hot plasmas give good indications on the energy release distribution itself. Lee et al. (1995) have compared the soft X-ray peak flux and the hard X-ray fluence distribution. Different slopes are found, leading the authors to conclude that other heating mechanisms than energy deposited by accelerated electrons must act in flares.

The interpretation of the shape of the frequency distributions has been investigated in the literature and basically two classes of models ('stochastic relaxation' and 'avalanche model') have been developed (see Sect. 5.2). Assuming that the total energy contained in non-thermal electrons or hot plasmas is correlated to the total energy released during a flare, the observed distributions can be confronted to the predictions of these models. This has been done for hard X-ray flares with an energy range between 10^{28} to 10^{33} ergs. However, very little information is known on the distributions of X-ray flare parameters for weaker events.

In this paper we present a new solar X-ray flare statistical study based on observations at photon X-ray energies above 10 keV recorded by the *Danish Wide Angle Telescope for Cosmic Hard X-Rays* (WATCH) experiment aboard the Russian spacecraft GRANAT. The energy release in these flares is estimated to lie below the range observed by ISEE-3/ICE or HXRBS/SMM. Frequency distributions are performed on the different measured X-ray parameters.

WATCH measures the X-ray flux in the deka-keV range for which few observations have been performed with scintillators. This experiment allows to make systematic observations in this intermediate zone between hard X-ray observations above 20 keV and observations in the soft X-ray thermal range (e.g. with GOES). In Sect. 2 the WATCH unit that observes the Sun (referred to as WATCH-0) is presented including a description

of how the energy calibration of the detector was performed. Thereafter (Sect. 3) the creation of the WATCH solar flare catalogue is explained and some examples of solar observations are given. For some of the solar events we discuss the possible interpretations of the radiation observed and an estimation of the energy content of the largest flares observed is given. Sect. 4 presents the different statistical studies that were performed on the WATCH solar database. In Sect. 5 the results of the statistical study are discussed in relation with previous studies and in the context of avalanche models. Sect. 5 furthermore summarizes the conclusions of the paper and discusses some prospective studies.

2. The WATCH experiment aboard GRANAT

The GRANAT satellite was launched on 1. Dec. 1989 and the WATCH experiment is composed of 4 WATCH units mounted in a tetrahedral geometry, each being designed with a very large field-of-view (4 steradians). One of the WATCH units has the Sun in its field-of-view and there exists almost two years of solar observation, covering the solar data gap between the end of the HXRBS/SMM observations (December 1989) and the launch of COMPTON (April 1991). As the GRANAT orbit is highly eccentric and has a long period ($\sim$96 hours), it allows long uninterrupted observations between passages through the radiation belts of the Earth. Telemetry was on an average done every 24 hours on 3 days out of 4 in each GRANAT orbit.

2.1. Technical description

The WATCH detectors are based on the rotation-modulation-collimator (RMC) principle which allows to get some information on the arrival direction of the photons. The first modulation collimator was designed by Oda (1965) and consisted of two plane grids of parallel wires separated by a short distance and placed in front of a detector. The Oda technique was thereafter improved by letting the two planes of parallel 50 % transmission grids rotate synchronously around a fixed axis perpendicular to the grids. This allows to modulate the X-ray flux received from a point source. This technique referred to as rotation-modulation-collimator (RMC) was proposed by Mertz (1968) and further developed by Schnopper et al. (1968, 1970) and Willmore (1970).

The WATCH experiment is based on the RMC-principle, but the second grid of the collimator has been replaced with two interleaved grids of X-ray detectors (NaI(Tl) and CsI(Na)) (Lund 1985). The advantage of this method is that by adding together the count rates in the two scintillators, the X-ray burst time profile can be measured, unaffected by the modulation pattern. The ratio between the count rate measured in one scintillator and the total count rate provides the normalized instrumental modulation pattern which can be extracted independently of the time variations in the source flux (Lund 1981). The interleaved scintillator grids of the WATCH detector are a circular mosaic of 22 scintillator (NaI and CsI) strips, each having a width of 5 mm and a thickness of 2 mm. The modulation grid is mounted 5 cm above the scintillator surface and is made up of rods of tantalum with an equal width and a spacing of 5 mm thus providing a spatial resolution of 5.7 °. To provide a sufficient mechanical strength of the grid as well as to absorb fluorescent X-rays produced in the tantalum, thin layers of copper and of carbon fiber epoxy were added to the tantalum grid. The total area of the detector system is 95.0 cm^2 equally divided between the NaI and CsI scintillators. The two scintillators are viewed by a single photomultiplier tube through a lead glas optical window and have an X-ray entrance window of 25 micron Aluminium which prevents optical light from entering the scintillator and allows the X-rays to pass with little absorption above 6 keV. The signals from the two types of scintillators can be separated electronically, due to the different decay characteristics of the scintillator materials (0.23 μs for NaI(Tl) and 0.63 μs for CsI(Na)).

For the study of solar bursts, basically two count rate channels and two modulation channels from the NaI scintillator were used. The time accumulation for the count rates and modulation patterns is based on the rotation velocity of the modulation grid/scintillator system which is slightly variable with time but which is recorded. The time accumulation for the normal count rate data is approximately 6.5 seconds (8 rotations) and for the modulation patterns approximately 13.9 minutes (1024 rotations). Bursts (triggers) having rise times less than two rotations causes the WATCH instrument to enter burst mode. The accumulation time for the count rate is of one rotation, approximately 0.8 seconds. For bursts triggers with time scales of 2 to 32 seconds the observing program enters the transient mode. In this mode modulation patterns with 16 rotation time accumulation are collected ($\sim$ 13 seconds).

2.2. The WATCH modulation pattern

When the modulation and scintillator grid of WATCH rotate together, the illuminated fraction of the scintillator will vary as (Brandt 1994):

Eq. (1): $\triangle$= saw[((πL)/d) tan(θ) cos(x-ϕ) + δ]

where saw[ ] is the symmetric triangle sawtooth function normalized between 0 and 1 with period 2π (saw(0)= saw(π)= saw(2π)=0.5, saw(π/2)= 1 and saw(3π/2)=0.0), L is the distance between the modulation grid and the scintillator surface, d is the width of the tantalum rods of the grid, x is the rotation phase in radians [0,2π], θ is the off-axis angle of the source in the WATCH field-of-view (the angle between the rotation axis and the incident radiation), ϕ is the phase angle of the source within the field-of-view (the spin axis of the solar viewing WATCH unit on GRANAT is located in the symmetry-plane of the satellite's solar panels and as a consequence the solar image never deviates much from the ϕ=0 line in the field-of-view). δ is the measure of the relative position of the grid and assembly of the scintillator strips in units of π/d (δ= 0 corresponds to half of each scintillator strip being exposed when the instrument is illuminated head-on). For WATCH on GRANAT δ is approximately equal to 0. In reality the modulation grid is not infinitely thin and the

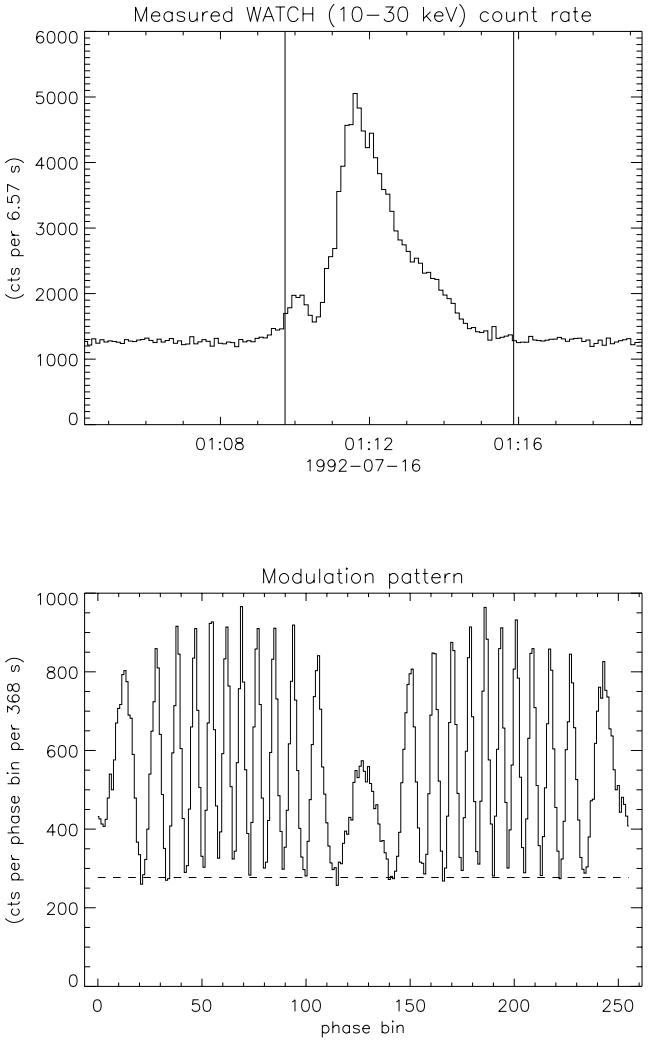

Fig. 1. The time profile of a solar event (top) with corresponding modulation pattern (bottom). The background estimated in the countrate time profile before and after the burst is indicated as a dotted line in the modulation pattern.

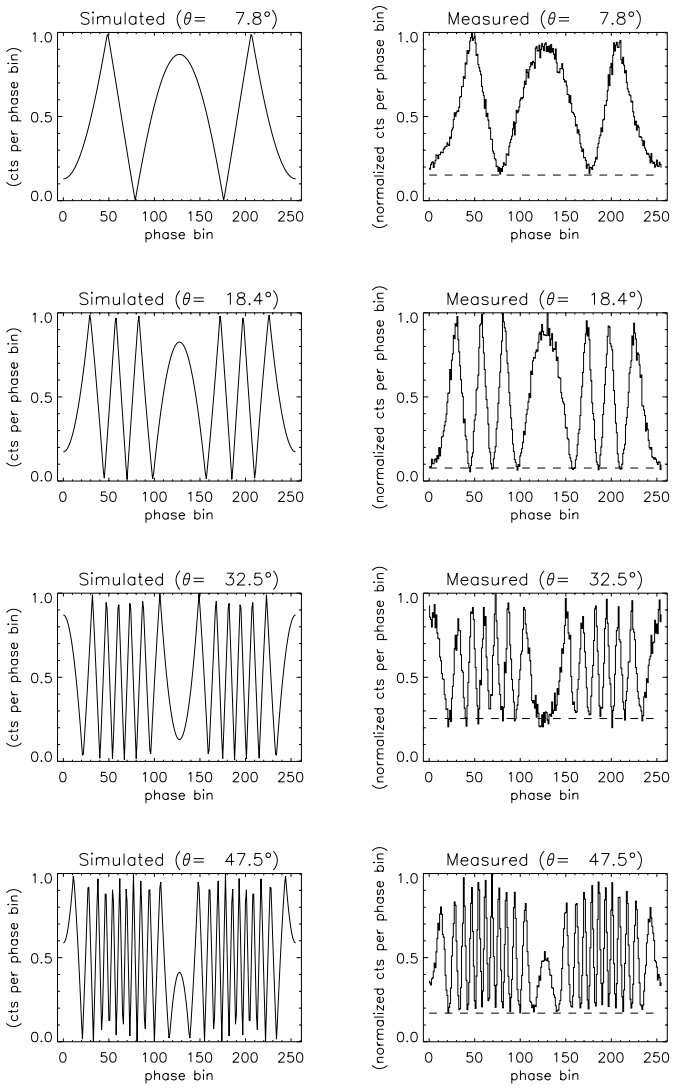

Fig. 2. The simulated solar modulation pattern (left) for different incident angles compared with the measured solar modulation patterns normalized to the maximum countrate. The background measured in the countrate time profiles before or after the burst is indicated as a dotted line.

finite thickness of the grid must be taken into account when attempting to model the shadow pattern. For a detailed analysis of how the real modulation pattern was simulated, see Brandt (1994).

One rotation is divided into 256 equal angular increments. Thus the modulation patterns consist of 256 values of count rates that are integrated over a given accumulation time. They are used in determining the positions and strengths of the X-ray sources in the field-of-view. The upper part of Fig. 1 shows the time profile of a solar event in the 10-30 keV energy range. The modulation pattern has been accumulated over the time indicated by the two vertical lines. The modulation pattern (bottom) is centered at phase bin= 128 (ϕ= $\sim$0) as expected for the Sun. Fig. 2 illustrates how the simulated solar modulation pattern (left side) using Eq. 1 compares with the observed modulation patterns normalized to the maximum count rate (right side) for different incident angles θ. It can be noticed that for all incident angles θ, the modulation pattern for the Sun is always centered at phase bin 128 (ϕ= 0). The other X-ray sources will be identified by their different modulation patterns (as e.g. the Crab Nebula).

2.3. Energy calibration of the NaI scintillator

Before launch the WATCH experiment was calibrated using radioactive sources. However a major gain shift after launch prevents us from using this prelaunch calibration. Furthermore, the radioactive source (Cd-109) associated with each detector was found to be too weak compared to the background to be used for calibration after launch. Therefore the energy calibration of the WATCH-0 detector was performed in the following way: 1) Modelling the detector and 2) Using observations of the Crab Nebula source for the energy calibration. The purpose of the

energy calibration is not to perform a complete spectral analysis but to get an estimate of the energy bands in which count rates were accumulated and of the number of photons corresponding to a given count rate.

The X-ray detection efficiency depends on the X-ray absorption coefficients of the scintillators and the transparency of the Aluminium entrance window. The detection efficiency of the NaI scintillator in WATCH-0 is computed by using an analytic calculation of the energy loss probabilities in the detector (program developed by R.A. Schwartz, private communication). It takes into account the probability of photoelectric effect, Compton scattering and fluorescent escape in the scintillator as well as "broadening" due to the spectral resolution of the scintillator. The effect of the final thickness of the modulation grid for an incident photon with angle θ is to reduce the effective area by a factor g(θ) compared to the geometric projected area. Simulations of the mean value of the modulation patterns as a function of θ give the following correction factor: g(θ)= 2$\times$(0.5-0.121$\times$tg(θ)) for 2.90 °$<\theta<$ 51.80 °. Also included in the computation is the absorption by the Aluminium window and the thermal blanket located in front of the WATCH instrument. This blanket reduces the transmission efficiency of incoming photons. Before launch it was found that the transmission of 5.9 keV X-rays with blanket was about 60 percent of the transmission without the blanket. An indirect way of taking into account this passive material in front of the instrument is by multiplying the Aluminium thickness by a factor which compensates for this decrease in transmission efficiency. It was found that a value (f) of 1.63 gives a good estimate of the total transmission efficiency at 5.9 keV.

The simulation of the scintillator is then performed using the previous description. The electronic chain of the detector amplifies the output signal of the scintillator with a certain gain which changed during the 2.5 years of the observations (Castro-Tirado 1994). This implies that the effective energy ranges of the count rate channels changed during this period in relation with the changes of the gain. To determine the effective energy channels of WATCH-0, a standard X-ray source must be used. During the 2.5 years of observation the Crab Nebula was at times in the field-of-view. Its coordinates in relation to the orientation of the experiment are known, so that one can identify this source in the background by its modulation pattern. The low- and high-energy count rates can thus be calculated using the two corresponding modulation patterns. It is found that the Crab count rates in WATCH-0 changed over the 2.5 years simultaneously to the changes of the voltage of the experiment (from May 1991 to November 1991). After this period, the voltage returned to its previous value. Three observing periods must then be defined corresponding to different values of the WATCH-0 energy channels.

For each period the Crab incident photon spectrum given as:

Eq. (2):dN/d(hν)= $2.02\cdot10^{-2}\times$(hν/20)$^{-2.09}$
ph cm^{-2} s^{-1} keV^{-1} with hν in keV

Table 2. Effective energy ranges of WATCH-0

Observing Period	Low-Energy (keV)	High-Energy (keV)
Dec. 1989 - March 1991	10 - 30	>30
April - Nov. 1991	14 - 40	>40
Dec. 1991 - July 1992	10 - 30	>30

is introduced into the response of the detector. The count rates produced in the low- and high-energy channels are computed for different limits of the output energy bands and compared with the observed count rates. The effective energy ranges found from this procedure are indicated in Table 2.

The knowledge of the effective energy ranges of the channels allows to estimate the number of counts that will be registered in each given channel. The right side of Fig. 3 illustrates for periods 1 and 3 the expected count rates for a non-thermal photon spectrum I(hν)= A$\times$(hν/10)$^{-\gamma}$ with A=1 and hν is the energy of the incoming photons in keV. The harder the spectrum (the lower the spectral index γ) the more counts are expected in the high-energy channel and the lower the ratio between the two channels. The left side of Fig. 3 shows for periods 1 and 3 the expected count rate as a function of temperature (T) for a given thermal photon spectrum I(hν) defined by the temperature T of the emitting plasma and its emission measure (EM) with EM= 10^{47} cm^{-3}. For low temperatures, count rates are recorded mainly in the low energy channel. With increase in temperature the expected number of counts will increase much faster in the high-energy channel compared with the low-energy one.

3. Observations

The WATCH solar burst catalogue (Astronomy and Astrophysics Supplement Series) was created by systematically going through the WATCH-0 database with the following selection criteria:

1) The modulation pattern must correspond to the solar one (i.e. it must be centered at $\phi\sim$0, see Sect.2.2.2).

2) There must be a signature in the GOES data (a classified GOES flare or a significant flux enhancement). The corresponding WATCH peak is not necessarily at the same time as that of the GOES event. Note that in general this second criterium is redundant with the first one.

3) The peak count rate of the WATCH event must be above the three sigma background level.

4) The event must not be significantly contaminated by particles.

A total of 1551 events were found, where approximately 45 percent of the events are associated with GOES X-ray flare classification (607 C-flares, 84 M-flares and 2

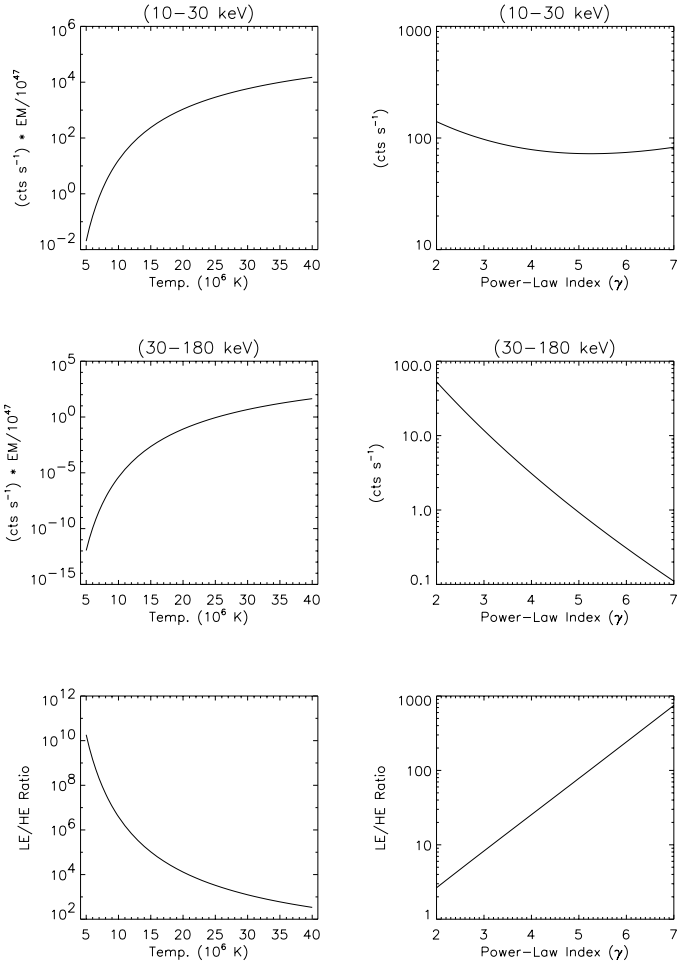

Fig. 3. Right side: The expected count rates in the low and high energy channels and the ratio for a non-thermal spectrum as function of the spectral indices. Left side: The expected count rates in the low and high energy channels and their ratio for an incident thermal photon spectrum as a function of temperature (see text for details).

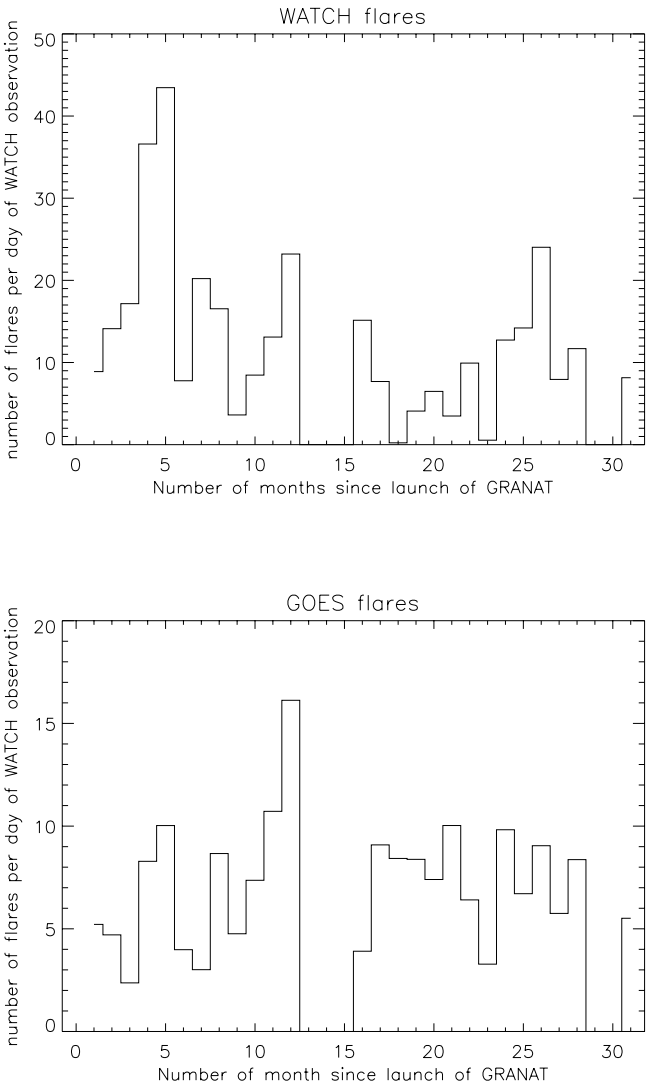

Fig. 4. Top pannel: The monthly flaring rate recorded by WATCH-0. Bottom pannel: The corresponding monthly flaring rate recorded by GOES.

X-flares). 27 of these events were observed to have signals above background in both the low- and high-energy channels.

Furthermore, each WATCH solar burst was tentatively associated with an active region with the following selection criteria:

- the WATCH event is associated with a reported GOES flare associated with an active region in Solar Geophysical Data (comprehensive reports).

- the WATCH event is not associated with a reported GOES flare, but is simultaneously detected with an optical flare. The X-ray burst may begin a few minutes before the optical flare ending either during or after it, or it may begin during the optical flare and end before it. Only one optical flare must occur at the same time as the WATCH event for the association to be considered as valid.

A more detailed description of all the parameters accompanies the catalogue.

The top pannel of Fig. 4 shows the flaring rate as deduced from the WATCH-0 observations, where the on-time (total duration of WATCH observations for the month) is computed in days. The bottom pannel is the flaring rate as deduced from GOES. The flaring rate recorded by WATCH in the second observing period (month 16 to 23) decreases as expected from the shift of the energy channels described in Sect. 2.3.

3.1. Solar X-ray bursts observed by WATCH

The bottom of Fig. 5 shows the time profile recorded in the low-energy channel of WATCH on the 19 June 1990 between 15:00 and 16:20 UT (the dotted line represents the background). The two upper pannels of the figure show complementary GOES observations in two energy channels (the dotted line also represents the background - see below in Sect. 3.2). No signal above background is observed in the high-energy channel of WATCH. The first burst (a) observed at peaktime 15:23:24 UT is associated with an optical flare and some significant GOES emission,

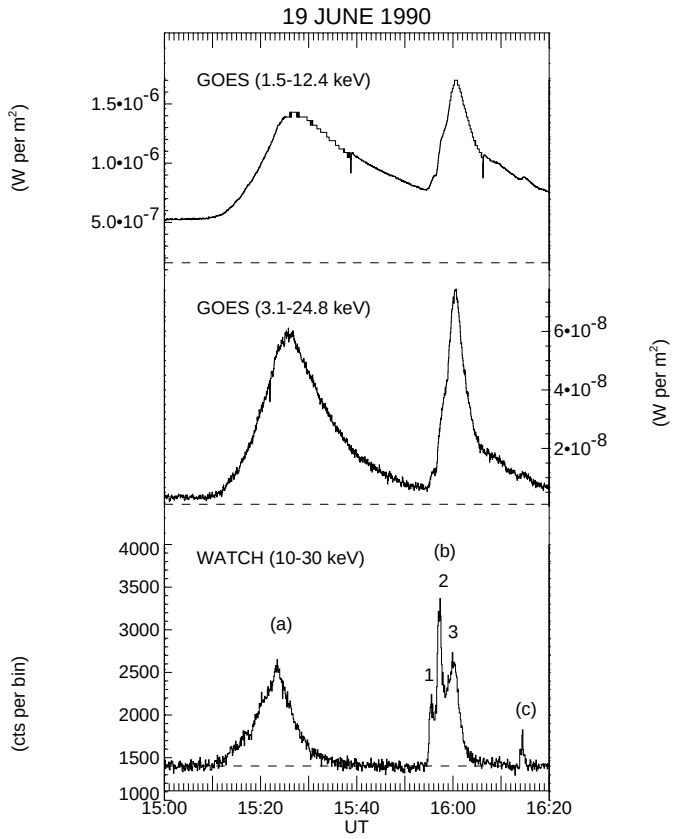

Fig. 5. Time profiles of the three WATCH bursts (bottom) observed between 15:00 and 16:20 UT on 1990 June 19 with the corresponding GOES time profiles (see text for details).

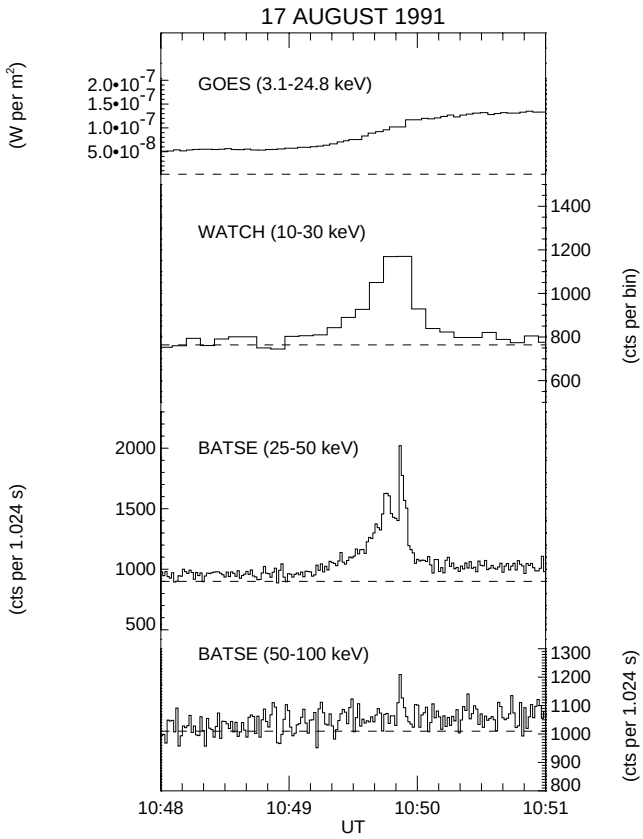

Fig. 6. Time profiles of a burst (1991 August 17) observed simultaneously by WATCH and BATSE in the rising phase of a GOES flare.

which is however not reported as a GOES flare in 'Solar Geophysical Data'. The two bursts that follow (peaktimes: 15:57:16 UT (b) and 16:14:26 UT (c)) are both associated with a C1.6 GOES flare and a common optical flare. The first two peaks (1 and 2) in the burst (b) are seen as bumps in the GOES time profile, whereas the third peak (3) is close to the peak of the event observed at lower energies by GOES. Note that for this burst as for others the peak count rate as well as the peak time indicated in the WATCH catalogue corresponds to the largest peak detected in the low-energy channel of WATCH (here peak 2).

For some events, complementary observations at energies above 25 keV have been found originating e.g. from the Burst and Transient Source Experiment (BATSE) aboard the Gamma-Ray Observatory (GRO) (Fishman et al. 1989). The WATCH event presented in fig. 6 corresponds to an impulsive non-thermal weak and short duration burst also observed with BATSE in the rising phase of the GOES flare. However no signal in the high-energy channel of WATCH was observed, probably because of the smaller detector area of WATCH compared to BATSE.

3.2. Nature of the Deka-keV emission observed by WATCH

As a first investigation of the nature of the emission observed by WATCH above 10 keV, it is checked whether the emission results only from the contribution of the thermal plasma measured by GOES. Fig. 7 is a schematic representation of how this was done.

Assuming that the emission measured in the two GOES soft X-ray ranges (1.5-12.4 keV and 3.1-24.8 keV) is produced by a homogeneous isothermal plasma, those observations are used to determine the parameters (temperature and emission measure) of this soft X-ray emitting plasma. Formulae relevant for the GOES-1 satellite data have been derived by Thomas et al. (1985). However a significant difference in detector efficiencies between the experiments aboard the different GOES satellites has been found by Sylwester et al. (1995), who have derived conversion factors between the different experiments. Following the suggestion by Garcia (1994), the GOES wavelength-averaged efficiencies given by Sylwester et al. (1995) are used to convert the GOES-7 fluxes into GOES-1 fluxes before they are used in the formulae of Thomas et al. (1985).

Two methods are used to determine the pre-event background of the GOES flux observations. 1) A rough estimation of the pre-event flux level which represents an upper limit of the background level. 2) The technique developed by Bornmann (1990) which determines the background by stating that the

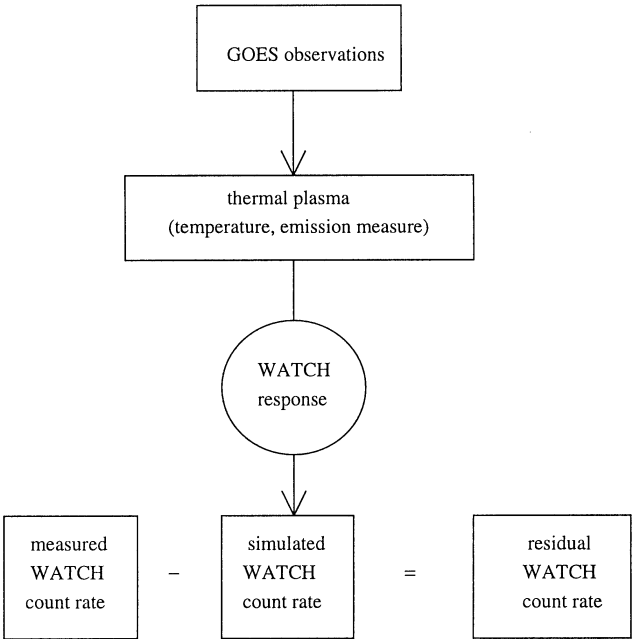

Fig. 7. A schematic representation of the simulation of the combined WATCH and GOES observations.

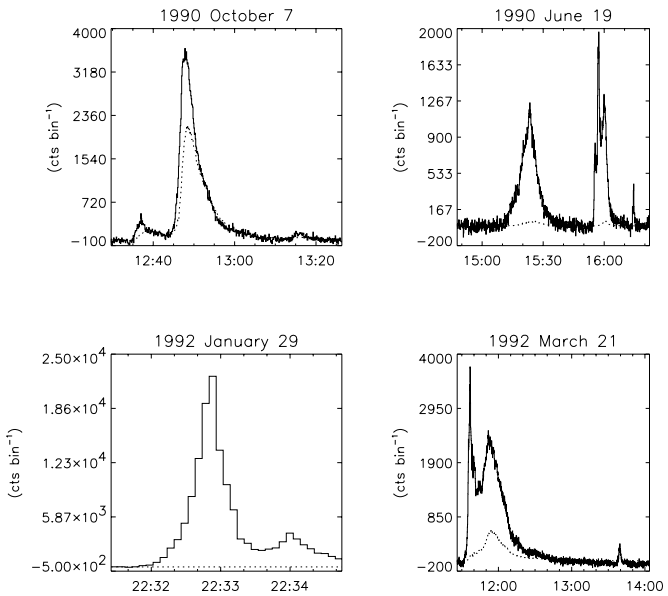

Fig. 8. Measured (full line) and simulated (dotted line) WATCH count rates for four different events (see text for details).

temperature, emission measure and flux should all increase at the start of the soft X-ray brightenings and that the flaring X-ray sources is hotter than the average of all background sources. It is found that the background levels and thus the temperatures and emission measures determined with the above two methods are consistent.

The temperature and emission measure inferred from GOES give an estimate of the thermal spectrum impinging on the WATCH detector as a function of time. Using the detector response that was described in the previous section, it is then possible to simulate the time evolution of the WATCH count rate produced by the thermal plasma. For all cases that were analyzed, the simulated count rate was always smaller than the observed one indicating that, as expected, the emission cannot be represented by an isothermal plasma alone. The simulated time profile is then subtracted from the measured WATCH count rate and what is left over is called the 'residual' (Fig. 7). Fig. 8 shows the measured count rate in the low-energy channel (full-line) compared with the simulated one (dotted line) for four events. In Fig. 8a-c the simulated count rates represent respectively 50 %, 20 %, ∼0 % of the detected count rate. The ratio between the detected and simulated count rates thus vary from one event to the other. It may also vary a lot in the course of a burst (as for the 21-03-1992 burst in Fig. 8d) and is found to be generally higher at the rise phase of a burst. This confirms either the usual multithermal nature of the flaring plasma or shows the frequent production of suprathermal electrons. It also confirms the variation from one burst to the other or even in the course of a burst of the relative contribution of hot plasmas or of suprathermal electrons.

In some cases (see Fig. 8a) up to 50 % of the low-energy count-rate of WATCH can be produced by the contribution of the thermal plasma measured by GOES and no signature is detected in the WATCH high energy channel. In those cases, two models have been used to analyse the combined GOES and WATCH data (see Crosby et al. 1996 and Crosby 1996 for details and examples to reproduce the combined observations of WATCH and GOES). The first of this model is based on the assumption that the flaring plasma can be represented by two thermal components and the two sets of temperature and emission measure are determined using the following guidelines:

- the high temperature component must not give a significant signal in the high-energy WATCH channel.
- the low temperature component accounts for the low-energy GOES channel.
- both components account for the 3.1-24.8 keV GOES channel and the low-energy channel of WATCH.

This analysis has been performed for the two events discussed in Crosby et al. (1996) (see Table 3a) and it was found that the hot plasma could be represented by a temperature in the range of 1.1-1.4$\times 10^7$ K with an emission measure of 3-12$\times 10^{47}$ cm^{-3}, while the "cold" plasma had a temperature ranging between 5 and 7$\times 10^6$ K with an emission measure roughly ten times larger than the hot plasma. The temperatures of the hot plasma are found to be in the same range as those deduced by combined YOHKOH HXT and SXT observations (Hudson et al. 1994) for impulsive footpoint brightenings.

In some cases (e.g. the first peak of the 1992-03-21 event shown on Fig. 8d), the combined observations of GOES and WATCH cannot be reproduced by this above model (see also Crosby et al., 1996). The 'residual' in the low-energy WATCH channel must then be interpreted with the alternative model in terms of a non-thermal photon spectrum. In the following, this second model is used to analyse in a systematic way the

WATCH observations. The non-thermal spectrum is determined using the following constraints:

- the residual in the low-energy WATCH channel must be reproduced as well as the observations in the high-energy channel.
- if no significant emission is detected in the WATCH high-energy channel, only a limit of the photon spectral index is provided (see Table 3b) unless simultaneous observations of the event by other experiments are used to bring further constraints.

Table 3b summarize the results of the above analysis for the events studied in Crosby et al (1996) where no emission in the WATCH high-energy channel was observed and where simultaneous detection of the first peak of the 1992-03-21 event by BATSE was used as a further constraint. The results of the spectral analysis of all the WATCH events with significant flux in the high energy channels are similarly summarized in Table 4. Several peaks can be analyzed in these events, but we restrict ourselves to those for which no instrumental effects such as overflow, dead-time, or pulse pile-up are present. The slope of the non-thermal photon spectrum is found to be between -5.5 and -3.5 in agreement with values previously found in the literature in this energy range (Kane & Anderson 1970, Pan et al. 1984) as well as above 20 keV (Crosby et al. 1993; Bromund et al. 1995). The peak hard X-ray flux lies between 1 to 10 photons/(cm^2 s keV) at 20 keV for these events and is about one order of magnitude lower for the events studied in Crosby et al (1996) (Table 3b). These values lie towards the lower end of what was observed for HXRBS (Crosby et al. 1993). The peak energy flux in electrons above 25 keV is also computed assuming a thick-target model for the X-ray production. The values above 25 keV are found to lie around 10^{26}- 10^{27} ergs/s. Compared to the values found for the HXRBS observations (Crosby et al. 1993), the hardest bursts detected by WATCH correspond to an energy content at the lower limit or below the range detected by HXRBS. This suggests that the smallest and/or softest of the events detected by WATCH may belong to the same scale of events as the microflares detected by Lin et al. (1981).

Comparable time profiles sometimes observed around 10 keV with WATCH and at higher energy also suggest that the emission may be attributed to non-thermal origin even down to 10 keV. The Neupert effect generalized as the relationship between the time derivative of the soft X-ray time profile with the hard X-ray light curve (Dennis & Zarro 1993) is also observed in some cases between WATCH time profiles and the GOES ones around a few keV (Vollmer 1995). Fig. 9 illustrates such an example for an event where significant emission is observed in both channels of WATCH and a purely non-thermal photon spectrum has been derived (see Table 4). The correlation coefficient between the derivative of the two GOES channels with the low-energy channel of WATCH is found to be around 0.9, while it is around 0.76 with the high-energy channel of WATCH. This shows an apparent causal relationship between the soft X-ray emission observed by GOES and the deka-keV emission observed by WATCH. Such a causal relationship has

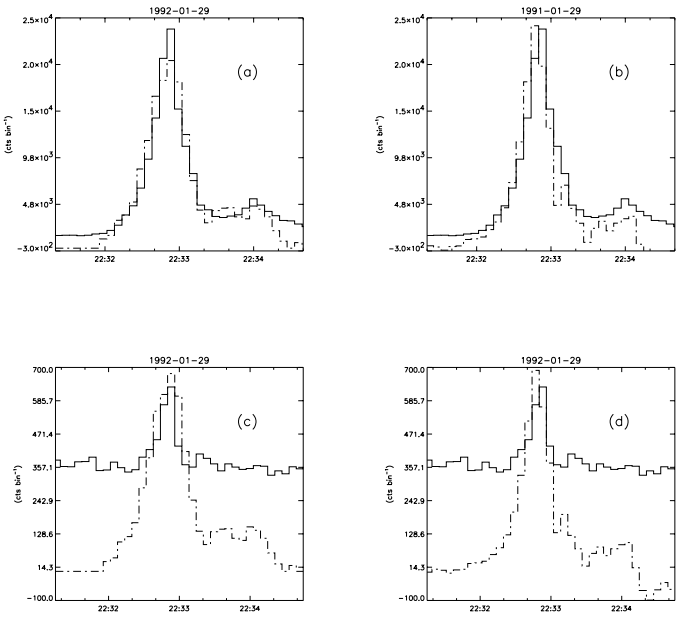

Fig. 9a–d. The derivative of the two GOES time profiles compared with the WATCH count rates for the 1992 January 29 event. The top two figures (**a** and **b**) represent the low-energy time profile of WATCH (full line) and the bottom two figures (**c** and **d**) the high-energy time profiles of WATCH (full line). The dotted lines are the derivatives of respectively the low-energy channel of GOES (right-side) and of the high-energy one (left-side).

been extensively studied at higher X-ray energies (e.g. Dennis & Zarro, 1993). A commonly proposed interpretation of this effect suggests that the non-thermal energetic electrons radiating hard X-ray emission are also at the origin of the heating and subsequent thermal bremsstrahlung observed in soft X-rays (e.g. Dennis & Zarro, 1993). It must however be pointed out that the relationship between the time profiles is not sufficient to support the causal relationship which must be further demonstrated by a comparison of the energy contained in the non-thermal electrons and radiated by the hot plasma. The present observations of a Neupert effect between the deka-keV and the lower energy time profiles may simply suggest that in some events the observations in the deka-keV range are a good indicator of the primary energy release in the flare and not of the thermal response of the medium. Thus the deka-keV X-ray energy range can be potentially used as a diagnostic of the flare energy release process.

3.3. Conclusions

The present section shows some examples of solar bursts observed by WATCH around 10 keV. Depending on the event or on parts of the event, the light curves resemble either those of the soft X-ray emission observed by GOES or those of the non-thermal hard X-ray emissions observed e.g. by BATSE. Several deka-keV WATCH events may be observed during a single GOES soft X-ray flare. The injection of energy above 10 keV occurs thus throughout a soft X-ray flare and not only at the

Table 3. Spectral analysis of the two WATCH events described in Crosby et al. (1996)

a) Thermal plasma with two components (peak values) (deduced from GOES and WATCH observations)

date	1990 Oct. 7 (12:47:45)		1992 March 21 (part II) (11:51:41)	
plasma	cold	hot	cold	hot
T (10^6 K)	5-7	12-13	5-6	11-14
EM (10^{47} cm^{-3})	29-24	12-7	133-97	16-3.1

b) Non-thermal electron spectrum (WATCH residual-peak values)

date	photon spectral index γ	A	peak hard X-ray flux at 20 keV (ph cm^{-2} s^{-1} keV^{-1})	peak energy flux $>$25 keV (ergs s^{-1})
1990 Oct. 7 (12:47:45)	$\geq$4.5	1.2×10^5	0.16	$\leq5.7\times10^{25}$
1992 March 21 (part I) (11:36:44)	$\sim$5.0	8.2×10^5	$\sim$0.26	$\sim9.5\times10^{25}$
1992 March 21 (part II) (11:51:41)	$\geq$4.5	1.4×10^5	0.20	$\leq6.8\times10^{25}$

Table 4. Spectral analysis of purely non-thermal events (observed in both energy channels of WATCH.

date	UT	photon spectral index γ	A	peak hard X-ray flux at 20 keV (ph cm^{-2} s^{-1} keV^{-1})	peak energy flux $>$25 keV (ergs s^{-1})
90/03/27	22:36:36	5.5	2.6×10^7	1.82	7.0×10^{26}
90/03/27	22:40:31	3.5	1.2×10^5	3.35	9.4×10^{26}
90/05/21	15:30:55	4.5	2.6×10^6	3.63	1.3×10^{27}
90/05/21	15:31:02	5.0	1.2×10^7	3.75	1.4×10^{27}
90/07/04	11:09:45	4.0	1.7×10^6	10.62	3.4×10^{27}
90/07/04	11:10:25	4.5	3.6×10^6	5.03	1.7×10^{27}
91/08/25	09:36:21	5.5	5.2×10^7	3.63	1.4×10^{27}
92/01/29	22:33:51	5.5	2.4×10^7	1.68	6.5×10^{26}
92/04/24	19:18:59	5.0	8.8×10^6	2.75	1.0×10^{27}

rise phase of the flare. This was sometimes observed at higher X-ray energies by HXRBS/SMM, but less systematically. A lot of small soft X-ray enhancements not classified as GOES flares are associated with small bursts observed by WATCH around 10 keV. The production of suprathermal populations or of hot components in the corona is thus not limited to the "usual" GOES soft X-ray flares classified in 'Solar Geophysical Data'. The spectral analysis performed on some events clearly shows that the emission around 10 keV does not only result from the plasma detected around a few keV by GOES. A hotter component or a non-thermal population is required in the solar corona to produce this emission. As already suggested from the previous analysis of a few flares (Hernandez et al. 1986, Kane et al. 1992), the non-thermal electron population thus extends down to 10 keV in many events.

4. Statistical analysis of solar X-ray flare parameters

4.1. Frequency distributions of X-ray flare parameters

Using the WATCH solar burst catalogue, frequency distributions are derived for the following parameters: peak count rate, total duration, rise time and decay time. Events where start, end/or peak time are not observed are not included (14 events) in the analysis, thus giving a total of 1537 events for the study.

4.1.1. Flare peak count rate frequency distribution

It is first investigated whether the shape of the frequency distribution of the flare peak count rate above background is sensitive to the shift in the energy bands of WATCH discussed in Sect. 2.3. It is found that the frequency distributions obtained for the different observing periods are all well-represented by power-laws above a turn-over with a slope which does not change significantly during the three observing periods.

The analysis can thus be performed on the total database and Fig. 10 (top) illustrates the frequency distribution of the peak count rate for the total database. It can be represented, above the turn-over at 50 c/s and for almost three orders of magnitude, by a power-law with a slope α, where α= -1.58 +/- 0.02.

We furthermore divided the events into five subgroups as function of their total duration (D): 6.5 s $<$ D $<$ 200 s, 200 s $<$ D $<$ 400 s, 400 s $<$ D $<$ 700 s, 700 s $<$ D $<$ 1000 s, D $>$ 1000 s. The frequency distributions are performed on the five subgroups and the two extremes are illustrated in Fig. 10 (bottom). All five frequency distributions can be represented by power-laws above a turn-over, but it is found that the slope of the power-law systematically varies with the range of durations of the events (see Table 5). The slope is steepest for the sub-group with the shortest duration and as the duration increases for each sub-group the slope of the power-law decreases. It must be noted that this effect is systematically observed independently of the values of the durations used for the limits of the sub-groups.

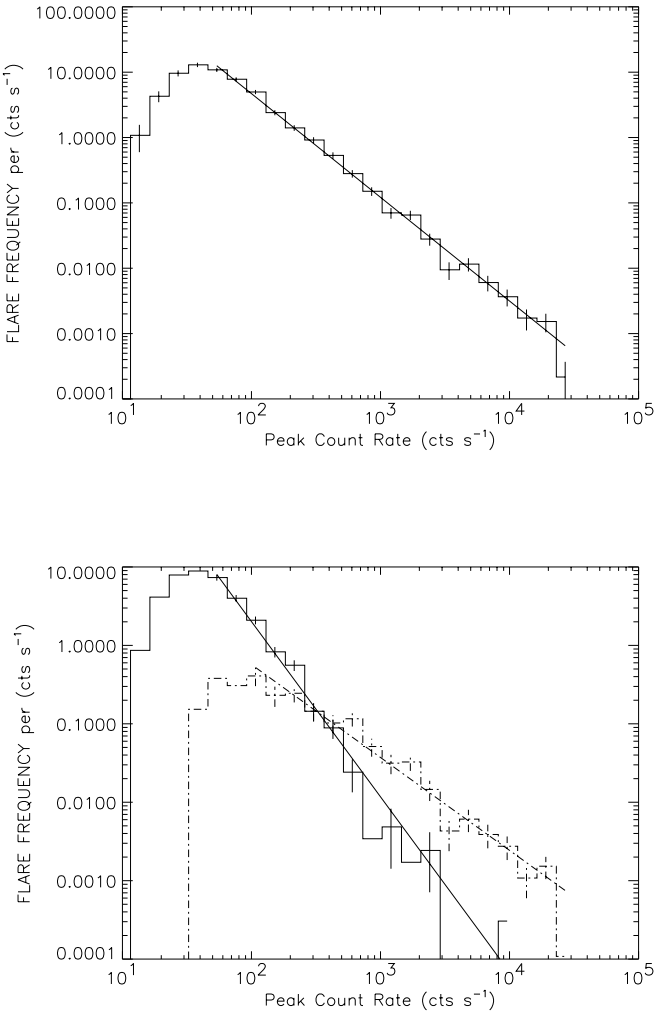

Fig. 10. The frequency distribution of the WATCH flare peak count rate for the total observing period (top) well-represented by a power-law above the turn-over at 50 c/s (1251 events) with a slope α= -1.58 +/- 0.02. The frequency distribution of the WATCH peak count rate for different sub-groups of events (bottom). The steeper slope (α= -2.17+/- 0.07) refers to events with duration less that 200 seconds (full line) and the flatter slope (α= -1.15+/-0.05) to events that have durations greater than 1000 seconds (dashed curve)

4.1.2. Total duration, rise and decay time frequency distributions

Fig. 11 represents the frequency distribution of the burst total duration for the whole database. A single power-law above a turn-over does not fit the distribution very well. This effect was already suggested in other databases (Crosby et al. 1993; Bromund et al. 1995), but is much more pronounced in the present study probably because of the longer day-time orbit of the spacecraft which allows to observe longer duration events. Double power-law representation or a power-law with an exponential roll-over as suggested by Lu et al. (1993) have been used to fit the distributions and the results are summarized in Tables 6 and 7. The events are then divided into subgroups defined by the range of peak count rates (P$<$100 c/s, P$>$100 c/s)

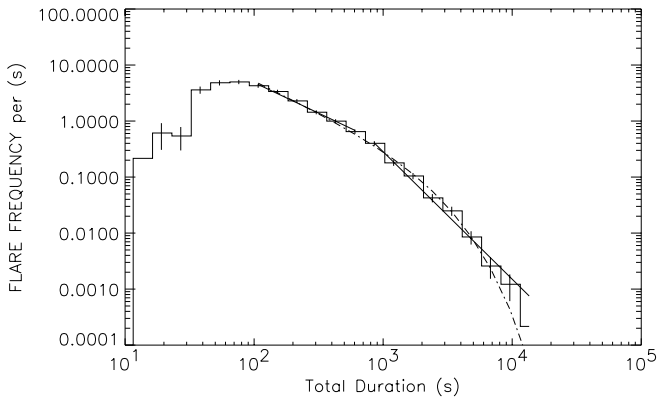

Fig. 11. The frequency distribution of the bursts total duration for the whole observing period, and the fitting by either a single power-law with a slope (γ= -1.08+/-0.03) with an exponential roll-over at T_{max}= 2100 +/- 100 s (dotted line) or by two power-laws with slopes: β_1= -1.09+/-0.05 and β_2= -2.28 +/- 0.08 (full lines).

Table 5. Characteristics of the frequency distributions in peak count rates for sub-groups of events.
N_{fit}: number of events in the fit
N_{tot}: total number of events in the distribution.

duration interval (seconds)	slope (α)	N_{fit}	N_{tot}
t>6.5	-1.58+/-0.02	1251	1537
6.5<t<200	-2.17+/-0.07	437	653
200<t<400	-1.82+/-0.08	236	309
400<t<700	-1.46+/-0.06	190	229
700<t<1000	-1.34+/-0.03	108	124
t>1000	-1.15+/-0.05	206	222

to investigate if the parameters of the frequency distributions vary from one sub-group to the other (see Tables 6 and 7). It is found that the distribution is always steepest in the long time range. When the frequency distributions are fitted by a single power-law with an exponential roll-over, the power-law is flatter for the sub-group with the largest peak count rates, while the value of T_{max} (s) defining the exponential roll-over systematically increases (see Table 7). A similar behaviour is obtained for frequency distributions of rise and decay times (see Crosby, 1996 for more details).

4.2. Correlation between the different X-ray flare parameters

Fig. 12 illustrates the correlation scatter plots between the different characteristic times (total duration, rise and decay time) as function of peak count rates. The slopes of the different correlation plots are similar ($\sim$0.5). The correlation coefficients range between 0.5 and 0.6, the coefficient between the peak

Table 6. Characteristics of the frequency distributions in total durations for subgroups of events (see text for details) (2 power-law fits).

	Total Duration	
	α_1	α_2
All events	-1.09+/-0.05	-2.28+/-0.08
P $<$ 100 c/s	-1.59+/-0.08	-3.15+/-0.35
P $>$ 100 c/s	-1.09+/-0.07	-2.67+/-0.17

Table 7. Characteristics of the frequency distributions in total durations for subgroups of events (see text for details) (power-law slope α with an exponential roll-over T_{max}).

	Total Duration	
	α	T_{max} (s)
All events	-1.08+/-0.03	2100+/-100
P $<$ 100 c/s	-1.28+/-0.06	800+/- 80
P $>$ 100 c/s	-0.90+/-0.11	2200 +/-150

count rate and the rise time being the lowest one (0.5). This is consistent with what was previously observed at higher X-ray energies with HXRBS/SMM (Crosby et al., 1993) where a loose correlation was also observed between the flare duration and the peak count rate.

4.3. Is there a relation between successive flares in the same active region?

A large percentage of the solar bursts recorded by WATCH could be associated with an active region. We define as $\triangle$T the elapsed time between two events in the same active region as the difference between the peaktimes of an event and of the preceding one. Bursts that are selected to define $\triangle$T must originate from the same telemetry dump or from adjacent dumps forming an uninterrupted sequence and be associated with the same active region. The study performed below on several active regions is based only on the dumps in which a lot of bursts arise from the same active region. (see Crosby (1996) for details). The frequency distribution of the elapsed time $\triangle$T is found to be well-represented by a power-law distribution with a slope (γ= -0.78 +/- 0.13) and an exponential roll-over (T= 19000 s +/- 5600). The slope is similar to what Pearce et al. (1993) found using the HXRBS/SMM database. The reason why the exponential roll-over was not observed in the HXRBS/SMM database may still be related to the fact that the SMM spacecraft had 60 minutes observation windows due to the low orbit. It is investigated whether the magnitude of bursts associated with the same active region is dependent or not on the time elapsed between successive bursts. The results are plotted in Fig. 13. No correlation is

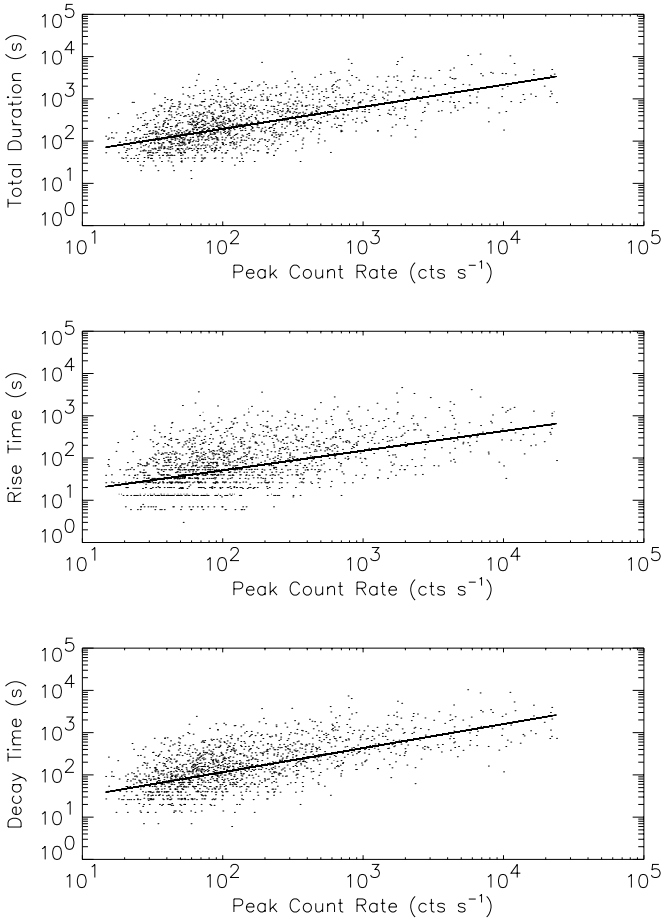

Fig. 12. Scatter plots between the (1) total duration, (2) rise time and (3) decay time with the peak count rate with the following slopes (s) and correlation coefficients (cc): (1) s= 0.52+/-0.07 and cc= 0.61, (2) s= 0.46+/-0.06 and cc= 0.50, (3) s= 0.57 +/- 0.06 and cc= 0.62.

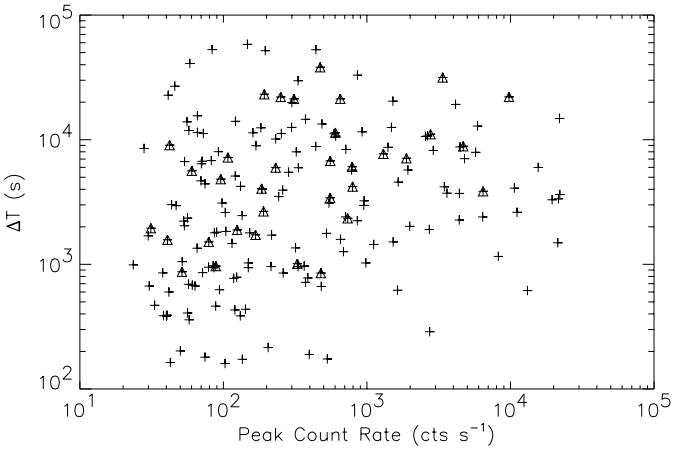

Fig. 13. Scatter plot between the elapsed time $\triangle$T since previous burst and the burst peak count rate for bursts associated with the same active region. This plot is obtained by the accumulation of 19 plots performed on several active regions. The triangles indicate that the preceding event had a large peak count rate (1000 c/s).

found between the elapsed time $\triangle$T and the size of the event. It is also checked whether $\triangle$T is dependent on the size of the preceding event. The triangles on Fig. 13 correspond to bursts for which the preceding event was larger than 1000 c/s. As can be noticed, there is no evidence of the need of a sufficient time interval for a burst (even a big one) to occur after a large burst in the same active region.

5. Discussion and conclusion

5.1. Energy contained in the WATCH flares

The analysis of the WATCH observations shows that in agreement with previous works, the X-ray emitting component around 10 keV does not only result from the plasma detected around a few keV by e.g. GOES. Either a hotter component or a non-thermal electron population must produce this emission. The similar time profiles observed around 10 keV and at higher energies suggest that non-thermal emission is produced in some events down to $\sim$10 keV. This has previously been suggested from the analysis of other flares in both soft and hard X-ray domains (e.g. Gabriel et al. 1984; Hernandez et al. 1986; Gabriel et al. 1991; Kane et al. 1992). In some events, there is an indication of a "Neupert effect" between the WATCH time profiles at 10 keV and the derivatives of GOES time profiles around a few keV. This suggests that X-ray emission around 10 keV contains indeed a non-thermal component, and thus is a good indicator of the primary energy release in a flare.

Assuming non-thermal emission for the most energetic deka-keV bursts observed by WATCH, it is found that the peak energy flux extrapolated to the HXRBS/SMM range is that of the small hard X-ray flares (less than 10^{27} ergs/s above 25 keV). This suggests that the complete WATCH solar database discussed in this paper deals with smaller energy releases than those observed by HXRBS/SMM.

The observations of solar bursts by WATCH also revealed that several bursts at 10 keV may occur during a single GOES soft X-ray flare. This suggests that the injection of energy contained in suprathermal electrons occurs throughout a flare and not only at the rise phase of this flare. A lot of small soft X-ray enhancements detected by GOES are associated with small bursts observed by WATCH around 10 keV. The production of a hot (T$\sim 10^7$ K) plasma in the corona or of a suprathermal population of electrons is thus a relatively common process, which is not only limited to GOES soft X-ray flares of class C or greater.

5.2. Frequency distributions and their interpretations

The earliest attempt to account for the flare size distribution was proposed by Rosner & Vaiana (1978) in the context of the 'stochastic relaxation model'. It is based on the following three assumptions: 1) flaring is a stochastic relaxation process, 2) the energy build-up is exponential between flares, 3) all the free energy built-up between flares is released by the following flare and the system returns to its unperturbed or ground state via flaring. In the case where the built-up energy exceeds the ground-state energy, these assumptions lead to a power-law fre-

quency distribution of released energies. In the simplest form of this model, some relationship is expected between the energy released in a flare and the time elapsed since the previous flare produced in the same flaring volume. This has been tested with WATCH observations with the result that no such relationship exists.

The more recent type of model to account for frequency distributions is based on the concept of self-organized criticality (SOC) also known as 'avalanche concept' introduced by Bak et al. (1988, 1989) and Bak & Chen (1991). This concept characterizes the behaviour of dissipative systems containing a large number of elements interacting over a short range, that evolve to a critical state in which a minor event starts a chain reaction that can affect any number of elements in the system. Frequency distributions of the output (size) parameters from the chain reaction taken over a period of time can be represented by power-laws. Lu & Hamilton (1991) proposed a model based on SOC, in which a solar flare is considered as avalanches of many small reconnection events. The frequency distributions of peak flux and total energy released are found to be well-fitted by power-laws with respective slopes -1.8 and -1.4 (Lu & Hamilton 1991). More recently Lu et al. (1993) further developed their model and found that a power-law with an exponential roll-over is a better representation for the frequency distributions. They have compared the predictions of the 'avalanche' models with the ISEE-3/ICE observations and have found a general good agreement between the predicted distributions of flare parameters and the observed ones. Their simulations also predict that there is no correlation between the size of an avalanche and the time interval since the previous one (Lu et al.,1993). This is confirmed in this paper with WATCH observations. All these observations are thus consistent with the 'avalanche' models of flares.

Further developments of the 'avalanche model' were done by Galsgaard (1995), Vlahos et al. (1995), and Georgoulis & Vlahos (1996) who either investigated the conditions of the system under which the energy release distributions are expected to be power-laws or the effects of the driving mechanism and of the instability and relaxation criteria on the slopes of the flare parameters occurence distributions.

Although, the energy range probed by WATCH may contain several emitting components, the statistical study performed on the WATCH database leads to results generally similar to those obtained on other databases at higher photon energies dealing with non-thermal emission. As was observed with HXRBS/SMM, there is a loose correlation between the total duration and the peak count rate of an event. The slope of the correlation line between the total duration and the peak count rate is found to be 0.52+/-0.07, in relatively good agreement with what was found with the HXRBS/SMM data (0.45+/-0.03) (Crosby et al. 1993).

The frequency distribution of the peak count rate above background can be represented by a power-law distribution for almost three orders of magnitude with a slope -1.58 +/- 0.02. The value of the slope differs slightly from the ones deduced from other experiments. This is probably due to the fact that the peak count rates are detector and energy dependent. Investigating the frequency distribution of the peak count rate for subgroups of events with different durations, we find that they are still well-represented by power-law distributions over several decades, while the slope systematically decreases with increasing duration. Such a behaviour is being currently modelled in the context of the "avalanche models" (Georgoulis et al., in preparation).

The total duration frequency distribution cannot be well represented by a single power-law. Although such an effect was already noticed in the HXRBS/SMM distributions (Crosby et al. 1993) and the ISEE-3 distributions Bromund et al. (1995), it is clearly seen in the WATCH observations, probably because of the larger detection of events with longer duration. The frequency distribution can be represented by two power-laws or by a single power-law (γ= -1.08 +/- 0.03) with an exponential roll-over (T_{max}=2100 +/- 100 s). The value of T_{max} is found to be close to what Lu et al. (1993) found comparing numerical simulations of avalanches and ISEE-3 observations of X-ray emission above 20 keV. This indicates a maximum duration of flares above which the single power-law behavior of the occurence distribution breaks down. This may indicate a limit in duration of a flare above which the dynamic evolution of the system is no longer governed by a self-organized behaviour. As suggested by Lu et al. (1993) the exponential roll-over value may also be related to the size of the flaring volume. It may suggest that small flares need smaller flaring volumes while the largest and longest flares originate from larger flaring regions (up to the size of an active region). If the events are divided into sub-groups as function of peak count rate, the power-law is flatter for the sub-groups with the largest peak count rates. This behaviour is currently being investigated by Georgoulis et al. (in preparation).

Even though the peak count rate around 10 keV is not an absolute measurement of the amount of energy released in a flare, it does offer some idea of the magnitude of the flare. Therefore the fact that there is no correlation between the strength of a X-ray flare and the elapsed time since the previous X-ray flare in the same active region questions the energy storage model of Rosner & Vaiana (1978) which assumes that energy is stored exponentially and is entirely released during the following flare. The observation that there is no strong link between the strengths of successive X-ray flares (associated with the same active region) is more consistent with the "statistical flare" models.

5.3. Conclusion and perspectives

The deka-keV energy range is one of the least studied energy ranges for solar purposes. The work presented here however indicates that non-thermal electrons are observed as low as 10 keV. Therefore it is of particular interest to study this energy range ($\sim$10 keV) in future, especially with higher spectral resolution. It should indeed provide clues to better estimate the energy released in the corona by the weak and numerous bursts which seems to be frequently observed in this photon range.

Furthermore the statistical results presented here show that the 'avalanche models' may provide a good context to under-

stand the frequency distributions of solar flare parameters. However some new observational results in this paper such as the deviations from single power-law distributions and the variation of slopes in subgroups of events must now also be explained in this context. No correlation is found between the elapsed time interval between successive flares arising from the same active region and the peak intensity of the flare. This raises questions on the energy storage model of Rosner & Vaiana (1978) and provides some support to the statistical flare models.

Acknowledgements. The authors thank Ms. K. Tolbert and Dr. R.A. Schwartz (Solar Data Analysis Center at Goddard Space Flight Center) for providing the GOES soft X-ray data on behalf of the US National Geophysical Data Center and the Solar Data Analysis Center at Goddard Space Flight Center. We are grateful to Dr. R.A. Schwartz who kindly provided us with a program allowing to compute the energy loss probabilities in a scintillator. This paper has also used data obtained through the CGRO BATSE Solar Flare Data Archive maintained by the Solar Data Analysis Center at NASA-Goddard Space Flight Center and provided by the BATSE team headed by Dr. G. Fishman. N.B. Crosby wants to thank the Commission of the European Communities (Human Capital and Mobility Program), the Danish Space Board and the Conseil Régional de la Région Centre for financial support. This work was supported by the GdR 132 of CNRS.

The authors would finally like to thank Dr. M.J. Aschwanden for his fruitful comments on the manuscript.

References

Bai T., 1993, ApJ, 404, 805
Bak P., Chen M., 1991, Sci. Amer., 46
Bak P., Tang, C., Wisenfeld, K., 1988, Phys. Rev., A38/1, 364
Bak P., Chen K., Creutz M., 1989, Nature, 342, 780
Biesecker, D.A., 1994, Ph.D. thesis, University of New Hampshire, USA
Biesecker D.A., Ryan J.M., Fishman, G.J., 1994, AIP Conference Proceedings, 294, 183
Bornmann P.L., 1990, ApJ, 356, 733
Brandt, S., 1994, Ph.D. thesis, Copenhagen University Observatory, Denmark
Bromund K.R., McTiernan J.M., Kane S.R., 1995, ApJ, 455, 733
Castro-Tirado A.J., 1994, Ph.D. thesis, Copenhagen University Observatory, Denmark
Crosby N.B., Aschwanden M.J., Dennis B.R., 1993, Solar Phys., 143, 275
Crosby N., Vilmer N., Lund N., Klein K.-L., Sunyaev R., 1996, Solar Phys., 167, 333
Crosby N.B. 1996, Ph.D. thesis, Observatoire de Meudon, France
Datlowe D.W., Eclan M.J., Hudson H.S., 1974, Solar Phys., 39, 155
Dennis B.R., Zarro D.M., 1993, Solar Phys., 146, 177
Dennis B.R., 1985, Solar Phys., 100, 465
Drake J.F., 1971, Solar Phys., 16, 152
Fishman G.J., Megan C.A., Wilson R.B., et al., 1989 in W. Neil Johnson (ed), Proceedings of the Gamma-Ray Observatory Science Workshop, Goddard Space Flight Center, 2
Gabriel A., Bely-Dubau F., Sherman J.C., Orwig L.E., Schrijver J., 1984, Adv. Space Res., 4(7), 221
Gabriel A., Bely-Dubau F., Millier F., 1991, AdV. Space Rs., 11, 323
Galsgaard K., 1995, A&A, 315, 312
Garcia, H.A., 1994, Solar Phys., 154, 275
Georgoulis K., Vlahos L., 1996, ApJ, 469, L135
Hernandez A.M., Machado M.E., Vilmer N., Trottet G., 1986, A&A, 167,77
Hudson H.S., Peterson L.E., Schwartz D.A., 1969, ApJ., 157, 389
Hudson H.S., Strong K.T., Dennis B.R., et al., 1994, ApJ, 422, L25
Kane S.R., Anderson K.A., 1970, ApJ., 162, 1003
Kane S.R., McTiernan J., Loran J., et al., 1992, ApJ., 390, 687
Kucera T.A., Dennis B.R., Schwartz R.A., 1997, ApJ., 475, 338
Kurt V.R., 1990, Basic Plasma Processes on the Sun, eds E.R. Priest, V. Krishan, 409
Lee T.T., Petrosian V., McTiernan M., 1993, ApJ, 412, 401
Lee T.T., Petrosian V., McTiernan M., 1995, ApJ, 448, 915
Lin R.P., Schwartz R.A., Pelling R.M., Hurley K.C., 1981, A&A, 251, L109
Lin R.P., Schwartz R.A., Kane S.R., Pelling R.M., Hurley K.C., 1984, ApJ, 283, 421
Lu E.T., Hamilton R.J., 1991, ApJ, 283, 421
Lu E.T., Hamilton R.J., McTiernann J.M., Bromund K.R., 1993, ApJ, 412, 841
Lund N., 1981, Ap. & S.S., 75, 145
Lund N., 1985, in Culhane J.L. (ed.), X-Ray Instrumentation in Astronomy, SPIE, 597, 95
Mertz, 1968, Fox J. (ed), Proceedings of the Symposium on Modern Optics, 17, Polytech. Inst. of Brooklyn
Oda M., 1965, Appl. Opt., Vol. 4, No. 1, p. 143
Pan L.D., Lin R.P., Kane S.R., 1984, Solar Phys. 91, 345
Pearce G., Rowe A.K., Yeung J., 1993, Ap&SS, 208, 99
Rosner R., Vaiana G.S., 1978, ApJ, 222, 1104
Schnopper H.W., Thompson R.I., Watt S., 1968, Space Sci. Rev., 8, 534
Schnopper H.W., Bradt H.V., Rappaport S. et al., 1970, ApJ, 161, L161
Schwartz R.A., Dennis B.R., Fishman G.J., et al., 1992, NASA CP-3137, 457
Shimizu T., 1994, Proceedings of Kofu Symposium, NRO Report No. 360, 61
Shimizu T., 1995, Publ. Astron. Soc. Japan, 47, 251
Sylwester J., Garcia H.A., Sylwester B.: 1995, A&A, 293, 577
Thomas R.J., Starr R., Cranell C.J., 1985, Solar Phys., 95, 323
Vlahos L., Georgoulis M., Kluiving R., Paschos P., 1995, A&A, 299, 897
Vollmer, B., 1995, rapport de stage, Observatoire du Meudon
Willmore A.P., 1970, MNRAS, 147, 387